Cosmiclike domain walls in superfluid ^{3}He-B: Instantons and diabolical points in $(\mathbf{k},\mathbf{r})$ space

M. M. Salomaa
Low Temperature Laboratory, Helsinki University of Technology, SF-02150 Espoo 15, Finland

G. E. Volovik
L. D. Landau Institute for Theoretical Physics, U.S.S.R. Academy of Sciences, 117334 Moscow, U.S.S.R.
(Received 10 April 1987; revised manuscript received 22 October 1987)

The possible planar superfluid B-B boundaries between inequivalent B-phase vacua are considered; such B-B interfaces provide an analogy with the cosmic domain walls that are believed to have precipitated in the phase transitions of the early Universe. Several of them display nontrivial structure in $(\mathbf{k},\mathbf{r})$ space (i.e., the union of the momentum and real spaces). Such a wall represents an instanton connecting two B-phase vacua with different $\mathbf{k}$-space topology. The transition between the vacua occurs through the formation of a pointlike defect either in the $(\mathbf{k},\mathbf{r})$ space, or in the $(\mathbf{k},t)$ space. These defects are so-called diabolical points of codimension 4, at which the fermionic energy tends to zero, thus providing the fermionic zero modes. Such points are new examples (within condensed-matter physics) of the peculiar diabolical points, which are characterized by the occurrence of a contact between the different branches of the quasiparticle spectra; in the present case, the branches of particles and holes, respectively. These points are here discussed for the case of the superfluid phases of liquid ^{3}He in close analogy with the quantum field theory of fermions interacting with classical bosonic fields. The cosmiclike domain walls in superfluid ^{3}He-B are observable in principle; in particular, the motion of the superfluid A-B interface is governed at low temperatures by the periodical emission of these topological excitation planes. The edges of B-B interfaces serve to generate fractionally quantized pure and mixed mass and spin supercurrent vortices in ^{3}He-B, while holes in these surfaces may give rise to the corresponding vortex rings and combined vortex and/or spin-disclination rings.

I. INTRODUCTION

The superfluid phases of liquid ^{3}He provide systems with the maximal known broken symmetries in the field of condensed-matter physics.[1] Consequently, a large number of different stable nonuniform structures for the order-parameter field—nonuniform vacua—can exist in these extraordinary condensed states of matter, which share not only the properties of superfluids and liquid crystals, but also those of ferromagnets and antiferromagnets. Some of these structures are extremely stable due to topological constraints: topological charge-conservation laws prohibit them from transforming continuously into the uniform vacuum state.[2] There may occur many different topological types for such configurations, which may be classified in terms of the homotopic groups that describe the continuous mappings of different parts of real space into the vacuum manifold.

The most important groups describing topologically stable configurations in superfluid ^{3}He are the so-called relative homotopy groups $\pi_n(\mathcal{R},\tilde{\mathcal{R}})$, where $\mathcal{R}$ and $\tilde{\mathcal{R}}$ denote vacuum manifolds in neighboring length scales. Since the hierarchy of interactions in ^{3}He implies a corresponding distribution of length scales [for instance, the coherence length (ξ_{GL}, where GL denotes Ginzburg-Landau); the dipole length (ξ_D); the magnetic length (ξ_H); etc.], the variety of the different possible types of topological configurations is quite numerous. Consider, for example, the singular defects: pointlike, linear, and planar; the nonsingular configurations (solitons) in the form of lines which may terminate at a point, or in the form of surfaces which may display an edge on a line; the defects on the surface of the liquid, boojums, etc. Moreover, configurations belonging to the same given topological type and possessing specific topological invariant(s)—*charge*(s)—may, nevertheless, yet differ from each other not only in internal symmetry,[3] but also, owing to their topology in the momentum space ($\mathbf{k}$ space), i.e., the topology of the zeros (nodes), in the energy gap on the Fermi surface[4,5] for the fermionic excitations.

These zeros of the energy gap—which correspond to the diabolical points of the fermionic quasiparticle spectrum where the intersection of the positive and negative branches of particles and holes occurs (see Sec. V for details and references), thus providing fermionic zero modes—are instrumental for the dynamics of superfluid ^{3}He. This plays a crucial role in the contacts between ^{3}He physics (in addition to the nontrivial topological configurations) with cosmology and particle physics growing stronger: near these nodes (here the diabolical points have the so-called codimension equal to 3, see Sec. V), the dynamics of the fermions interacting with the bosonic order-parameter fields share many features in common with the quantum-field theory of massless chiral Weyl fermions coupled to photons, W bosons, and gravitons, including the chiral anomaly,[6] in particular.

Here we consider yet another variety of

configurations—domain walls in ^{3}He-B, which belong to the trivial class within real-space topology. Although there prevails no topological stability, several distinct locally stable solutions of the Ginzburg-Landau equations (due to the complicated vacuum manifold that allows the existence of different symmetry classes of domain walls) even for the trivial topological class occur here. Essentially, the stability of the domain walls is provided by their symmetry, since in order to transform a wall from one symmetry class to another one involves the violation of symmetry in all of the intermediate states; the latter can be accompanied with an activation-energy barrier between the states.

Some of these solutions display distinct topology in **k** space: the domain walls connect two different **k**-space vacua, possibly with unequal topological invariants in the momentum space, thus representing instantons.[7] These instantons prove to provide examples of the diabolical points displaying the new codimension 4, near which the fermionic excitations are analogous to the Dirac fermions, in contrast with the Weyl fermions encountered in the case of diabolical points possessing codimension 3. According to contemporary cosmological ideas, analogous domain walls between inequivalent vacua may also have been created in the course of the phase transitions of the early Universe.[8]

II. VACUUM STRUCTURE OF SUPERFLUID ^{3}He-B

The group which is broken in ^{3}He below the superfluid phase-transition temperature T_c into a pair-correlated triplet state with Cooper-pair spin $S=1$ and with the pair orbital momentum $L=1$ [for the zero-field phase diagram of ^{3}He in the (p,T) plane, see Fig. 13], is

$$\mathcal{G}=\mathrm{U}(1)\times\mathrm{SO}_3^{(S)}\times\mathrm{SO}_3^{(L)} . \tag{1}$$

Here the indices (S) and (L) refer to solid rotations in the spin and orbital spaces, respectively. The breaking of the rotation groups $\mathrm{SO}_3^{(S)}$ and $\mathrm{SO}_3^{(L)}$ produce the magnetic and liquid-crystal-like behavior for the ordered phases of liquid ^{3}He, while the broken U(1) gauge group is responsible for the superfluidity. The order parameter in superfluid ^{3}He is specified by the 3×3 complex matrix $A_{\alpha i}$, which transforms under the action of the symmetry group $\mathcal{G}$ in Eq. (1) as follows:

$$A_{\alpha i}\rightarrow e^{i\Phi}R^{(S)}_{\alpha\beta}R^{(L)}_{ik}A_{\beta k} , \tag{2}$$

here $R^{(S)}$ and $R^{(L)}$ represent orthogonal matrices of spin and orbital rotations.

The vacuum manifolds may be found by minimizing the bulk part (F_B) of the following Ginzburg-Landau (GL) functional

$$F=F_B+F_G , \tag{3}$$

with the bulk condensation-energy term

$$\begin{aligned}F_B=\int d^3r\,(&-\alpha A^*_{\alpha i}A_{\alpha i}+\beta_1 A^*_{\alpha i}A^*_{\alpha i}A_{\beta j}A_{\beta j}\\&+\beta_2 A^*_{\alpha i}A_{\alpha i}A^*_{\beta j}A_{\beta j}+\beta_3 A^*_{\alpha i}A^*_{\beta i}A_{\alpha j}A_{\beta j}\\&+\beta_4 A^*_{\alpha i}A_{\beta i}A^*_{\beta j}A_{\alpha j}+\beta_5 A^*_{\alpha i}A_{\beta i}A_{\beta j}A^*_{\alpha j})\,.\end{aligned} \tag{4a}$$

Above, $\alpha=N(0)(1-T/T_c)/3$, with $N(0)=m^*k_F/2\pi^2\hbar^2$ abbreviating the density of the ^{3}He states (m^* denotes the effective mass and k_F the Fermi momentum for the ^{3}He quasiparticles) for one spin projection at the Fermi level; the coefficients β_i of the fourth-order invariants are here taken within the weak-coupling approximation[1] (this in no way restricts the symmetry or momentum-space topology of the solutions, which is our primary concern below). The gradient energy in the Ginzburg-Landau functional is given by

$$\begin{aligned}F_G=\int d^3r\,(&\gamma_1\partial_i A_{\alpha j}\partial_i A^*_{\alpha j}+\gamma_2\partial_i A_{\alpha i}\partial_j A^*_{\alpha j}\\&+\gamma_3\partial_i A_{\alpha j}\partial_j A^*_{\alpha i})\,,\end{aligned} \tag{4b}$$

where for weak coupling the bending coefficients are all equal (strong-coupling corrections being small), and given by $\gamma_1=\gamma_2=\gamma_3=\gamma=7\zeta(3)N(0)[v_F^2/240(\pi T)^2]$.

The B phase of ^{3}He, ^{3}He-B, corresponds to a uniform solution of the GL equation possessing the symmetry

$$\mathcal{H}=\mathrm{SO}_3^{(J)} , \tag{5}$$

with $\mathrm{SO}_3^{(J)}$ denoting the group of combined spin and orbital rotations. The uniform vacuum state with the symmetry specified by Eq. (5) is represented, e.g., by the order parameter (below, $\beta_{ij\ldots k}$ abbreviates $\beta_i+\beta_j+\cdots+\beta_k$):

$$A^{(0)}_{\alpha i}=\Delta_B\delta_{\alpha i},\quad \Delta_B^2(T)=\frac{\alpha}{2(\beta_{345}+3\beta_{12})} . \tag{6}$$

All the other degenerate B-phase vacua may be obtained operating on Eq. (6) by individual elements of the group $\mathcal{G}$, thus,

$$A_{\alpha i}=e^{i\Phi}R^{(S)}_{\alpha\beta}R^{(L)}_{ik}A^{(0)}_{\beta k}=\Delta_B e^{i\Phi}R_{\alpha i} , \tag{7}$$

where $R_{\alpha i}$ refers to an arbitrary orthogonal matrix, corresponding to a relative rotation of the spin and orbital spaces. Thus the vacuum manifold of the B-phase subspace of states is the product of U(1) for the phase Φ and the SO_3 manifold for the relative rotation

$$\mathcal{R}=\mathcal{G}/\mathcal{H}=\mathrm{U}(1)\times\mathrm{SO}_3 . \tag{8}$$

This connected manifold allows no *topologically* stable domain walls; topologically stable walls can only appear if an additional interaction [such as the spin-orbital (dipole) interaction and/or the magnetic-field energy] is taken into account, which acts so as to reduce $\mathcal{R}$ into its subspace $\tilde{\mathcal{R}}$ for large distances. As a result, two different types of domain walls of topological origin can arise which correspond, respectively, to the groups $\pi_0(\tilde{\mathcal{R}})$ and $\pi_1(\mathcal{R})/\mathrm{Im}[\pi_1(\tilde{\mathcal{R}})\rightarrow\pi_1(\mathcal{R})]$, comprising the relative homotopy group $\pi_1(\mathcal{R},\tilde{\mathcal{R}})$ (see Refs. 2 and 9). Both

latter types of domain walls exhibit widths several orders of magnitude in excess of the coherence length ξ_{GL} (with $\xi_{GL}^2=\gamma/\alpha$) being determined by the tiny dipole forces.

III. VACUUM INTERFACES: NONTOPOLOGICAL DOMAIN WALLS

Here we consider the rigid domain walls, whose stability is not supported by topology. These are stationary solutions of the GL equations—with width on the order of ξ_{GL}—which describe the interfaces separating domains of ^{3}He-B with different orientations of the order parameter $A_{\alpha i}$ in Eq. (7), i.e., with different Φ and $R_{\alpha i}$. For a given nontopological wall, the mutual orientation of the order parameters in the domains is not governed by external or internal forces (such as the dipole interaction), as in the topological domain walls, but instead it is rather fixed through the solution itself.

In this section we first describe in full detail the types of walls to be considered: we explain the physical principles necessary for the existence of stable domain walls and we identify the symmetries of all the possible domain walls separating the distinct B-phase vacua; these results are summarized in Table I. We then consider the structures for each of these solutions; correspondingly, the results for the order-parameter amplitudes are presented in Fig. 1.

The reason for the possible existence of nontopological boundaries is related to symmetry only: to destroy such an interface, one must exert the violation of its symmetry throughout the intermediate states which separate the state with the domain wall from a uniform vacuum equilibrium state in the configuration space. (This occurs when the symmetry H_W of the wall is not a subgroup of the symmetry $\mathcal{H}=SO_3^{(J)}\times T\times P$ of the uniform state.) This may involve an activation barrier for the process—thus providing the local stability of the domain wall even within the trivial class of real-space topology.

TABLE I. The symmetries and energies for the different possible stationary B-B domain walls shown in Fig. 1 between the ^{3}He-B vacua at zero magnetic field. The groups $C_{2v}^{(J)}$ and $C_{\infty v}^{(J)}$ are given in the Landau-Lifshitz notation; the additional superscript (J) here means that the corresponding rotations are to be applied simultaneously both in the spin and orbital spaces. Time inversion is denoted by T; P is the symmetry operator for space inversion: the space inversion P, when combined with a rotation that transforms the left vacuum into the right one, conserves the state intact. Note that the boundaries 1, 6, and 7 all display continuous axial symmetry about the symmetry axis x, while the remaining four B-B interfaces (2 through 5) share only discrete symmetry. The energies are computed per unit area (ξ_{GL}^2) and measured in normalized units as in Fig. 2. The minimum energy for solution 7, equal to 5.470, is the sum of its constituent parts, walls 1 and 6, i.e.: 2.317 + 3.153. The energy of the saddle-point solution 7 with normal core $[A_{xx}(x=0)=A_{yy}(x=0)=A_{zz}(x=0)=0]$ is considerably higher: 6.863, prior to decay into its elementary building blocks—the pair of walls $C_\pi^{(S)x}e^{i\pi}$ and $C_\pi^{(S)x}$. The symmetry $Pe^{i\pi}$ of the saddle-point solution becomes spontaneously broken in the minimum-energy configuration (cf. Figs. 1 and 11). The change $\Delta N\equiv N(x=+\infty)-N(x=-\infty)$ in the topological invariant N [defined by Eq. (20)] on crossing through the wall is also given for each vacuum interface.

B-B interface	g	$gA_{\alpha i}^{(0)}/\Delta_B$	H_W: Symmetry of wall	Energy	ΔN
1	$C_\pi^{(S)x}e^{i\pi}$	$\begin{bmatrix}-1&0&0\\0&+1&0\\0&0&+1\end{bmatrix}$	$C_{\infty v}^{(J)}\times T\times PC_\pi^{(S)x}e^{i\pi}$	2.317	2
2	$C_\pi^{(S)y}e^{i\pi}$	$\begin{bmatrix}+1&0&0\\0&-1&0\\0&0&+1\end{bmatrix}$	$C_{2v}^{(J)}\times T\times PC_\pi^{(S)y}e^{i\pi}$	1.351	2
3	$C_\pi^{(S)z}e^{i\pi}$	$\begin{bmatrix}+1&0&0\\0&+1&0\\0&0&-1\end{bmatrix}$	$C_{2v}^{(J)}\times T\times PC_\pi^{(S)z}e^{i\pi}$	1.351	2
4	$C_\pi^{(S)z}$	$\begin{bmatrix}-1&0&0\\0&-1&0\\0&0&+1\end{bmatrix}$	$C_{2v}^{(J)}\times T\times PC_\pi^{(S)z}$	4.178	0
5	$C_\pi^{(S)y}$	$\begin{bmatrix}-1&0&0\\0&+1&0\\0&0&-1\end{bmatrix}$	$C_{2v}^{(J)}\times T\times PC_\pi^{(S)y}$	4.178	0
6	$C_\pi^{(S)x}$	$\begin{bmatrix}+1&0&0\\0&-1&0\\0&0&-1\end{bmatrix}$	$C_{\infty v}^{(J)}\times T\times PC_\pi^{(S)x}$	3.153	0
7	$e^{i\pi}$	$\begin{bmatrix}-1&0&0\\0&-1&0\\0&0&-1\end{bmatrix}$	$C_{\infty v}^{(J)}\times T\times Pe^{i\pi}$ $\Downarrow$ $C_{\infty v}^{(J)}\times T$	6.863 $\Downarrow$ 5.470	2

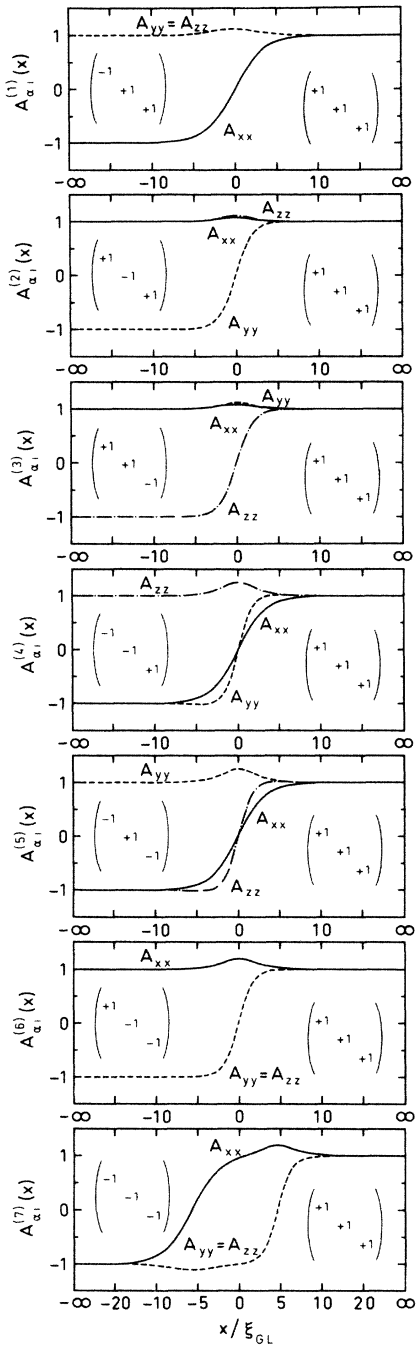

FIG. 1. The order-parameter $A_{\alpha i}$ variation for the seven inequivalent possible cosmiclike B-B domain walls in superfluid ^{3}He-B. Calculations were performed using the weak-coupling values for the five β parameters. The B-phase asymptote at $x=+\infty$ is fixed as $A_{\alpha i}^{(0)}(x=\infty)=\Delta_B\delta_{\alpha i}$. [This introduces no limitation on generality, since solutions with an arbitrary asymptote in Eq. (7) may be obtained from those found here through rotations in the spin space and/or via phase rotations.] The solid amplitudes denote $A_{xx}(x)$, dashed $A_{yy}(x)$, and the dashed-dotted $A_{zz}(x)$ between the vacuum states indicated in the figure (see also Table I). The position coordinate normal to the planar wall x is linear for $|x|<10\xi_{GL}$; for $|x|>10\xi_{GL}$ it varies as x^{-1}, to facilitate description of the complete axis: $-\infty\le x\le+\infty$. Distances are in units of the Ginzburg-Landau coherence length ξ_{GL}.

Let us find those kinds of distinct domain walls possessing trivial real-space topology, which can exist in ^{3}He-B. In the absence of external currents, a necessary condition for the existence of an isolated stable domain wall is the vanishing of mass and spin supercurrents *through the wall.* This provides crucial constraints on the mutual orientation of the order parameters on both sides of the wall. First, the change in the order-parameter phase Φ between the domains should be quantized in units of π: only in this case the phase difference generates no Josephson mass current through the wall. Likewise, the spin orientations in the domains should only differ by spin-rotation angles through $n\pi$ (with n an integer) in order to comply with the absence of a spin current normal to the wall. In the latter case, symmetry also dictates that the spin-rotation axis should be either normal to or within the plane of the wall.

As a result, we obtain the following group—which we denote here by $\bar{\pi}_0$—of the possible rotations and phase changes that may couple the two domains:

$$\bar{\pi}_0=\mathcal{Z}_2\times\mathcal{D}_2\ . \tag{9}$$

Above, $\mathcal{Z}_2$ means the subgroup $(e^{i\pi},1)$ possessing the two elements that describe the changes of phase through π and 0 (or 2π), while the subgroup $\mathcal{D}_2$ abbreviates the group $(1, C_\pi^{(S)x}, C_\pi^{(S)y}$, and $C_\pi^{(S)z})$ of spin rotations through π about the orthogonal axes $\hat{\mathbf{x}}$, $\hat{\mathbf{y}}$, and $\hat{\mathbf{z}}$. The $\hat{\mathbf{x}}$ axis is here chosen normal to the wall.

Rotation axes which are tangential to the wall may be chosen at will. However, if one considers combinations of several domain walls interacting with each other (described by the product group of the corresponding elements), symmetry requires either mutually parallel or perpendicular orientations for the rotation axes of the successive constituent walls. Therefore, one should only be limited by the existence of two tangential axes ($\hat{\mathbf{y}}$ and $\hat{\mathbf{z}}$).

There are seven nontrivial elements g constituting the group $\bar{\pi}_0$. Each element describes one of the seven different walls separating the states A and gA. The walls corresponding to the elements g are enumerated in Table I, where the reference ^{3}He-B vacuum-state order parameter A is chosen fixed as $A=A_{\alpha i}^{(0)}=\Delta_B\delta_{\alpha i}$. For the computed spatial variations of the order-parameter components in each of these vacuum interfaces, see Fig. 1.

The summation law for the fission and fusion processes of the domain walls is governed by the group multiplication table for $\bar{\pi}_0$. The isolated interfaces with minimal surface energy, $C_\pi^{(S)y}e^{i\pi}$ and $C_\pi^{(S)z}e^{i\pi}$, are degenerate in the free state since they may be obtained from each other through a combined rotation of the whole solution,

$$C_{\pi/2}^{(J)x}=C_{\pi/2}^{(S)x}C_{\pi/2}^{(L)x}\ . \tag{10}$$

However, when combined with the other walls, this degeneracy may be lifted owing to a mutual interaction. The pure phase wall $e^{i\pi}$ was previously discussed by Golo and Monastyrsky,[10] who considered the most symmetric possible form which necessitates a normal core state (with vanishing order parameter) in the wall. However, the solution for the $e^{i\pi}$ domain wall proves to be more in-

teresting (see Fig. 1): the superfluid state is restored at the expense of symmetry breaking (cf. Fig. 11); moreover, this state thus fissions into the composite of the two domain walls $C_{\pi}^{(S)x}e^{i\pi}$ and $C_{\pi}^{(S)x}$.

Figure 2 illustrates the distributions of the gradient and the condensation free-energy densities. Note that, up to a constant (i.e., the bulk equilibrium condensation energy), the functional forms are identical: $f_B(x)=f_G(x)$. This follows from "energy conservation:" consider replacing $x\rightarrow t$, where t is time. Then the Ginzburg-Landau functional becomes the Lagrangian $\mathcal{L}=F_G+F_B$; therefore, the conservation of "energy" E requires

$$E=f_B(x)-f_G(x)=\text{const}\ , \tag{11}$$

i.e., here the gradient energy F_G corresponds to the usual kinetic energy, while F_B is the analogue of potential energy. With an appropriate choice of $f_B(x)$ ($f_B\equiv 0$ for $t\rightarrow\pm\infty$), one ensures $E\equiv 0$, and hence $f_B(x)=f_G(x)$ is obeyed. This "virial theorem" is only valid for a one-dimensional inhomogeneity (such as the planar A-B and B-B boundaries), and cannot be generalized, e.g., to the case of vortices.

The general GL expression for the density of spin supercurrent in the direction (i) due to the αth component of magnetization is

$$j^{(i)}_{(\text{spin})\alpha}=-\varepsilon_{\alpha\beta\gamma}\,\text{Re}(\gamma_1 A^{*}_{\beta i}\nabla_j A_{\gamma j}+\gamma_2 A^{*}_{\beta j}\nabla_i A_{\gamma j} +\gamma_3 A^{*}_{\beta j}\nabla_j A_{\gamma i})\ , \tag{12}$$

where $\varepsilon_{\alpha\beta\gamma}$ denotes the Levi-Civita symbol. We find that there exist only two nonvanishing components of $\mathbf{j}_{(\text{spin})}$, in the directions $\hat{\mathbf{y}}$ and $\hat{\mathbf{z}}$, given by (in units of γ)

$$j^{(y)}_{(\text{spin})z}=-A_{xx}(x)\frac{\partial A_{yy}(x)}{\partial x}+A_{yy}(x)\frac{\partial A_{xx}(x)}{\partial x} \tag{13a}$$

and

$$j^{(z)}_{(\text{spin})y}=+A_{xx}(x)\frac{\partial A_{zz}(x)}{\partial x}-A_{zz}(x)\frac{\partial A_{xx}(x)}{\partial x}\ . \tag{13b}$$

Figure 3 displays distributions for the density of spontaneous spin supercurrents along the plane of the B-B vacuum interfaces.

Let us compare the properties of these solutions with those of topological solitons in the nontrivial class (element) of the relative homotopy group $\pi_1(\mathcal{R},\tilde{\mathcal{R}})$. There are two types of solitons, corresponding to the elements of the groups $\pi_0(\tilde{\mathcal{R}})$ and $\pi_1(\mathcal{R})/\text{Im}[\pi_1(\tilde{\mathcal{R}})\rightarrow\pi_1(\mathcal{R})]$. The planar solitons of the first group are undestroyable: they cannot possess an edge in the bulk, while the solitons of the second group can support an edge on linear topological defects (vortex, disclination, etc.) and, therefore, may be destroyed through the creation of a hole in the wall, see Fig. 4, bordered by a disclination loop[2,9] (these objects are called "walls bounded by strings" by Vilenkin[8]).

Our solutions share the properties of solitons in the second group. The sole difference is that the corresponding linear defect, which serves as the edge of the wall, is of nontopological origin. These defects are the following (see Fig. 5): half-quantum vortices (HQV's) for the $e^{i\pi}$

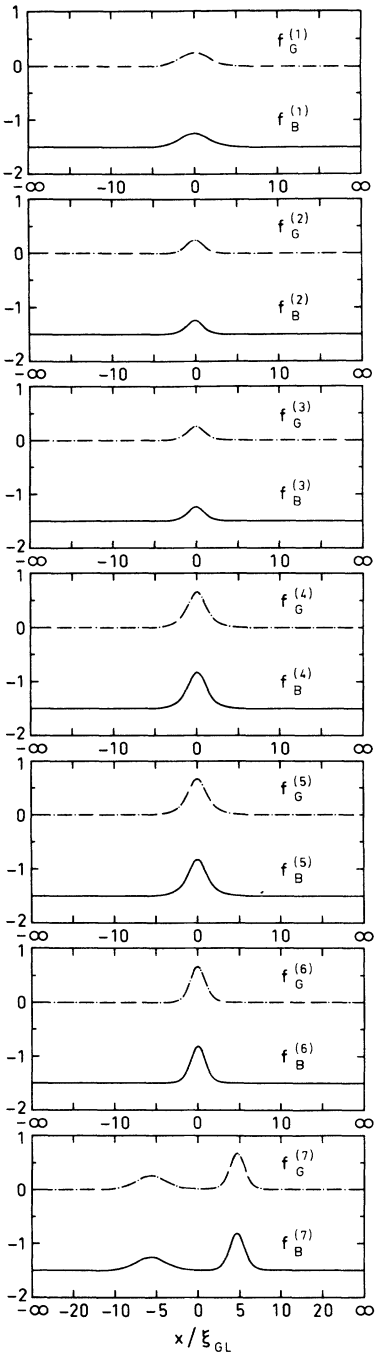

FIG. 2. Distributions of the gradient (f_G, dashed-dotted) and the bulk condensation energy (f_B, solid line) densities as functions of x, the position coordinate between the different B-phase vacua in Fig. 1. The equilibrium condensation-energy density in bulk ^{3}He-B is normalized to -1.5. Note that each of the domain walls feature a superfluid core [with nonvanishing condensation-energy density, $f_B(x)\neq 0$ for all x]; moreover, the curves fulfill the virial theorem [cf. Eq. (11)] with the functional form of the gradient energy (f_G) coinciding with that of the bulk condensation-energy density (f_B). Here the x axis is a truthful analogue to the imaginary time in an instanton describing the tunneling solution from one $\mathbf{k}$-space vacuum state into another one. Apparently, 7 does not qualify as a genuine solution but rather a composite object, having spontaneously disintegrated into the pair of walls, 1 and 6.

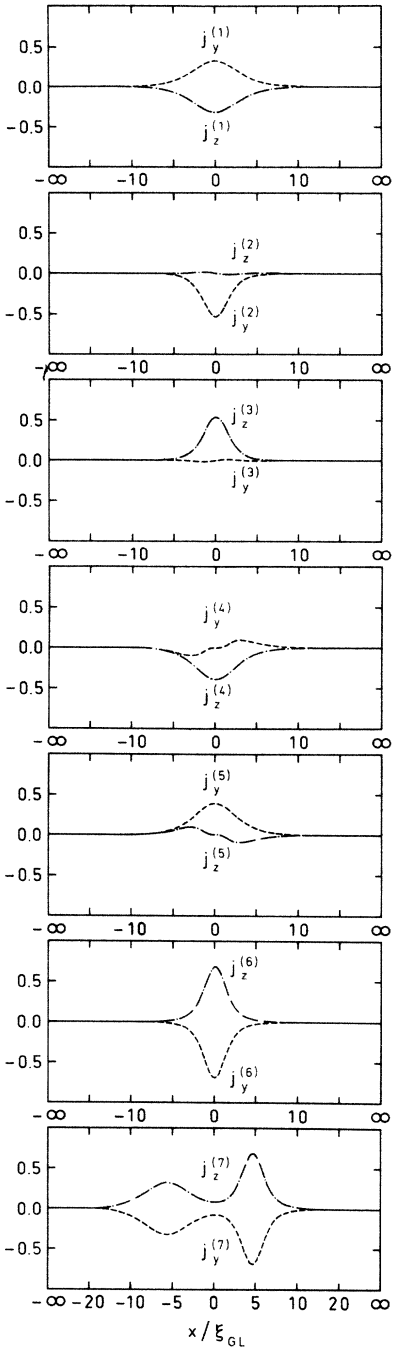

FIG. 3. All the solutions for the domain walls in ^{3}He-B found here have vanishing magnetization and they support no spontaneous mass supercurrents, even within the plane of the wall (due to time-inversion symmetry, owing to which the order parameter $A_{\alpha i}$ is real) but, nevertheless, they do display tangential spin supercurrents along the plane of the vacuum interfaces. Shown here are distributions of the components $j^{(y)}_{(\mathrm{spin})z}$ [Eq. (13a)]—denoted in the figure by j_y—and $j^{(z)}_{(\mathrm{spin})y}$ [Eq. (13b)]—denoted by j_z—for the spontaneous spin supercurrents in the plane of the B-phase vacuum interfaces of Fig. 1. Note the apparent mutual symmetries featured by the spin supercurrents for solutions 2 and 3—and those for 4 and 5—and the composite spin-supercurrent structure of solution 7=1 + 6.

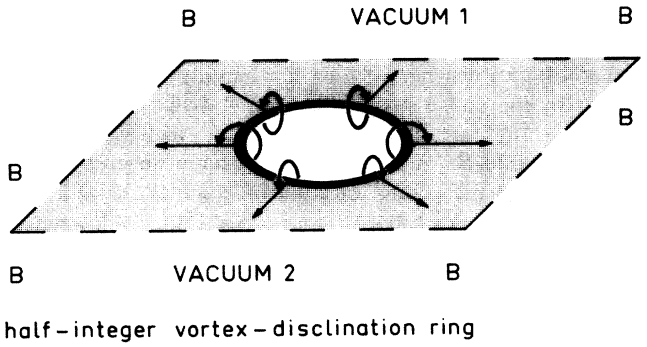

FIG. 4. The instanton between separate B-phase vacua can display a hole, bounded by a ring. Depending on the type of the domain wall, the ring will be a half-quantum vortex ring (for the $e^{i\pi}$ wall), a half-integer spin-disclination ring (e.g., for the boundary $C_\pi^{(S)x}$), or a simultaneous half-quantum vortex and a half-integer disclination ring (e.g., for $C_\pi^{(S)x}e^{i\pi}$). Once formed, and with its radius first exceeding several coherence lengths, the ring spontaneously expands out. While the ring propagates radially outward it serves to extinguish the domain wall.

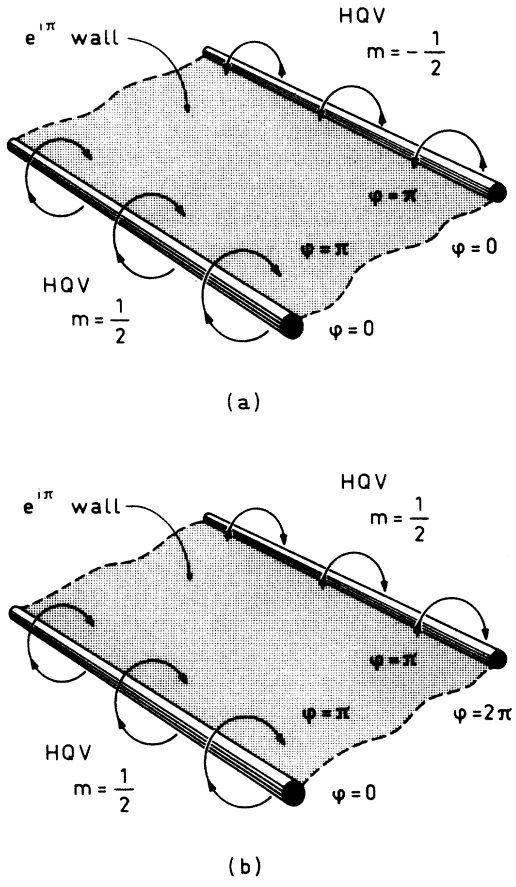

FIG. 5. The vacuum interfaces in ^{3}He-B represent planes of phase slippage, which may terminate in linear defects. Illustrated here are such edges of the domain walls involving half-quantum vortices (HQV) that carve the $e^{i\pi}$ domain wall from distinct B-phase vacua. (a) The two HQV's have opposite circulation: $m=\frac{1}{2}$ and $m=-\frac{1}{2}$. (b) The HQV's both share the same number of circulation quanta, $m=\frac{1}{2}$.

domain wall (in which the phase Φ changes by π), half-disclinations for the domain walls $C_\pi^{(S)x}$, $C_\pi^{(S)y}$, and $C_\pi^{(S)z}$, and combinations thereof for the remaining walls.

Due to the above properties, these structures can play an important part in the processes of phase slippage in superfluid ^{3}He-B: since a wall may have an end on the HQV's with the same circulation quanta $m=\frac{1}{2}$ and $m=\frac{1}{2}$ [see Fig. 5(b)], it could serve as a phase-slip center through $\Delta\Phi=2\pi$, leading to the dissipation of superflow. This structure closely resembles that of an extended vortex: the vortex core is spread out into a planar "sheet," whereas vorticity resides concentrated in the cores of the half-quantum vortices. The situation is analogous to quark confinement, with the half-quantum vortices corresponding to the quarks and the planar surface to the "glue" that holds them topologically confined. Note that the energetically most favorable walls, $e^{i\pi}C_\pi^{(S)y}$ and $e^{i\pi}C_\pi^{(S)z}$, and—related with them—the combinations of HQV's and half-disclinations serve for the simultaneous coupled dissipation of both mass and spin supercurrents.

IV. k-SPACE TOPOLOGY OF THE DOMAIN WALL: INSTANTON

Although the walls under consideration display no essential topological features in real ($\mathbf{r}$) space, some of them possess distinctive topology in the combined momentum ($\mathbf{k}$-) space and $\mathbf{r}$-space manifold, which serves to provide an instanton connecting the right and left vacua with different topological invariants in the $\mathbf{k}$ space. Topological defects in the $\mathbf{k}$ space are of paramount importance in the physics of superfluid ^{3}He, as well as in quantum electrodynamics: owing to the vanishing of the fermionic energy gap (zero modes) at the defects, they give rise to such effects common to ^{3}He and quantum electrodynamics like the screening of electric charge due to the polarization of the vacuum of chiral fermions and to the chiral anomaly. The equivalence of the ^{3}He dynamics near the $\mathbf{k}$-space defects and quantum electrodynamics originates from the same topological nature of these defects (see Sec. V).

Near the $\mathbf{k}$-space point defect, "boojum on the Fermi surface," which represents the diabolical point of codimension 3 (see Sec. V), where the energy gap for the ^{3}He quasiparticles tends towards zero, the dynamics of the fermionic quasiparticles coupled to the Bose fields of the order parameter is completely analogous to the dynamics of massless chiral fermions interacting with photons, W bosons, and gravitons within quantum-field theory, resulting in the chiral anomaly effects[6]—described by the very same equation as in the particle theory. As for ^{3}He-A and ^{3}He-B, the following examples serve to illustrate the importance of $\mathbf{k}$-space topology.

(i) Due to the $\mathbf{k}$-space defects, singular vorticity of the quantized vortex lines may be dissolved in such a manner that superfluidity is broken nowhere within the cores of the quantized vortices: The vortex singularity flares out from the real space into the $\mathbf{k}$ space,[4,5] thus facilitating a continuous distribution of vorticity in real space.

(ii) The creation of the gapless excitation governs the low-temperature dynamics of the topological objects, such as those of moving vortices, domain walls, instantons, etc.

Here the domain walls $e^{i\pi}$, $C_\pi^{(S)x}e^{i\pi}$, $C_\pi^{(S)y}e^{i\pi}$, and $C_\pi^{(S)z}e^{i\pi}$, for which there occurs a change through π of the phase factor for the ^{3}He condensate, are found to provide another example of the intercoupling of real-space and $\mathbf{k}$-space properties. The corresponding defect represents the diabolical point of codimension 4. Before the general discussion of these points (in Sec. V) within superfluid ^{3}He and quantum-field theory, let us first consider the topologies and structures of the order-parameter distributions in these walls. Here we need in the $(\mathbf{k},\mathbf{r})$ representation of the order-parameter field in superfluid ^{3}He, which is relevant in the Bogoliubov-Nambu Hamiltonian, describing the fermionic excitation dynamics. The corresponding Bogoliubov-Nambu matrix is as follows:

$$\hat{\mathbf{H}}(\mathbf{k},\mathbf{r})=\begin{bmatrix}\varepsilon_k & \Delta(\mathbf{k})\\ \Delta^\dagger(\mathbf{k}) & -\varepsilon_k\end{bmatrix}, \tag{14}$$

where $\mathbf{k}=(1/i)(\partial/\partial\mathbf{r})$ for the quantum problem; but in the semiclassical approximation, which is a good model for many physical situations, this $\mathbf{k}$ may be treated as a c number, with $\varepsilon_k=(k^2-k_F^2)/2m$ (where k_F denotes the Fermi momentum). The gap parameter $\Delta(\mathbf{k},\mathbf{r})$ is a symmetric 2×2 spin matrix for spin-triplet pairing and may be expressed in terms of the vector $\mathbf{d}$:

$$\Delta_{\alpha\beta}(\mathbf{k},\mathbf{r})=(g\sigma)_{\alpha\beta}\mathbf{d}(\mathbf{k},\mathbf{r}), \tag{15}$$

where the σ abbreviate the Pauli spin matrices and

$$g=\begin{bmatrix}0 & -1\\ 1 & 0\end{bmatrix}$$

is the metric spinor.

For the case of $L=1$ pairing, $\mathbf{d}$ is linear in the momentum $\mathbf{k}$, and it may be expressed in terms of the order-parameter matrix $A_{\alpha i}$ in Eq. (2) as follows:

$$d_\alpha(\mathbf{k},\mathbf{r})=A_{\alpha i}(\mathbf{r})\frac{k_i}{k_F}. \tag{16}$$

For the domain walls considered here, the vector $\mathbf{d}$ is real [this follows from the time-inversion (T) symmetry of the domain walls, see Table I]; it depends on $\mathbf{k}$ and x, and the energy of the fermionic excitations is in this case given by $E^2=H^2=\varepsilon^2+|\mathbf{d}|^2$. Let us consider the asymptotics on either side of the domain walls. For x tending to $+\infty$, we have fixed the limiting form corresponding to Eq. (6),

$$\mathbf{d}(\mathbf{k},+\infty)=\Delta_B\frac{\mathbf{k}}{k_F}, \tag{17}$$

while the asymptote for $x\to-\infty$ varies from one wall to another, e.g.,

$$\mathbf{d}(\mathbf{k},-\infty)=\Delta_B\left[-\frac{\mathbf{k}}{k_F}\right]\quad\text{for } e^{i\pi}, \tag{18}$$

while

$$\mathbf{d}(\mathbf{k},-\infty)=\Delta_B\left[\frac{\mathbf{k}-2k_x\hat{\mathbf{x}}}{k_F}\right] \quad \text{for } C_\pi^{(S)x}e^{i\pi}\,, \tag{19a}$$

correspondingly,

$$\mathbf{d}(\mathbf{k},-\infty)=\Delta_B\left[\frac{\mathbf{k}-2k_y\hat{\mathbf{y}}}{k_F}\right] \quad \text{for } C_\pi^{(S)y}e^{i\pi} \tag{19b}$$

and

$$\mathbf{d}(\mathbf{k},-\infty)=\Delta_B\left[\frac{\mathbf{k}-2k_z\hat{\mathbf{z}}}{k_F}\right] \quad \text{for } C_\pi^{(S)z}e^{i\pi}\,. \tag{19c}$$

On both sides of each wall one asymptotically has $|\mathbf{d}|=\Delta_B$ for $\mathbf{k}$ on the Fermi surface, i.e., the $\mathbf{d}$ field is defined on a sphere of radius Δ_B and it provides the mapping of the Fermi surface onto the $\mathbf{d}$ vector sphere with a nontrivial element of the group π_2:

$$N=\int_{\text{over Fermi surface}}\frac{dS_i}{8\pi\Delta_B^3}\varepsilon^{ikl}\mathbf{d}\cdot\left[\frac{\partial\mathbf{d}}{\partial k^k}\times\frac{\partial\mathbf{d}}{\partial k^l}\right]. \tag{20}$$

The topological charge N equals $+1$ for the right vacuum ($x=+\infty$), and $N=-1$ for the left one ($x=-\infty$) in any of the four domain walls involving a change of phase (in the other three B-B interfaces, $\Delta N\equiv 0$: there is no change in N). Thus the x axis acts as the time variable of the instanton, which serves to connect the $\mathbf{k}$ vacua with different topological invariants. Here the instanton is the point singularity in the $\mathbf{d}$ field (sometimes called a "hedgehog") in the three-dimensional $(\mathbf{k}/k_F,x)$ space, see Fig. 6, described by the homotopy group π_2.

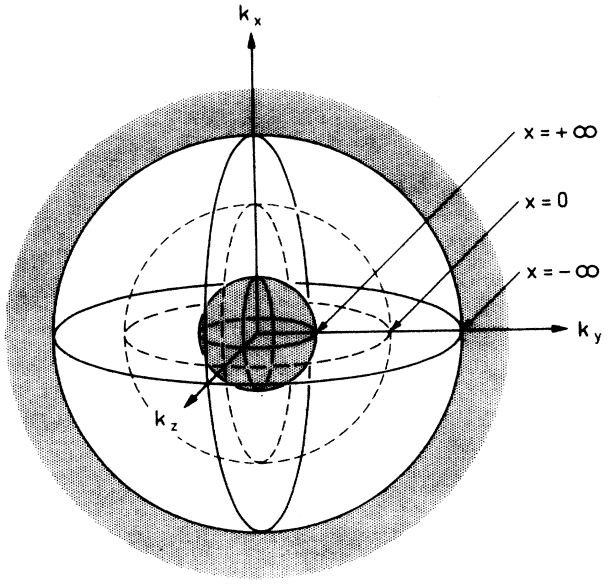

FIG. 6. The three-dimensional $(\mathbf{k},x)$ space is homeomorphic to a solid sphere enclosing a hole. The x-axis maps into r, the radial coordinate; the two-dimensional (2D) Fermi surfaces of $\mathbf{k}$ ($\mathbf{k}$ is restrained to lie on the Fermi sphere, and should thus be considered 2D) at each x maps onto a spherical surface with the corresponding r. For the mapping between the points $\mathbf{r}$ of the solid sphere and the coordinates $\mathbf{k}$ and x we use the relation $\mathbf{r}=(\mathbf{k}/|\mathbf{k}|)[1-\frac{1}{2}\tanh(x/5\xi_{\mathrm{GL}})]$, through Figs. 7–10 (in Fig. 11, x is scaled by $7.5\xi_{\mathrm{GL}}$).

Let us consider the instantons first on the example of a $C_\pi^{(S)x}e^{i\pi}$ wall. There are two such point singularities, each with $N=-1$: one at $x=0$, $\mathbf{k}=k_F\hat{\mathbf{x}}$ and the other at $x=0$, $\mathbf{k}=-k_F\hat{\mathbf{x}}$, see Fig. 7. For $x=+\infty$, the field $\mathbf{d}(\mathbf{k},+\infty)$ produces the mapping of the $x=+\infty$ spherical surface onto the $\mathbf{d}$-field sphere $S^2\to S^2$ with $N=+1$, while at $x=-\infty$, $\mathbf{d}(\mathbf{k},+\infty)$ gives the mapping with $N=-1$. The transition from one mapping to the other takes place through the formation of the two singular points on the Fermi surface at $x=0$, each with $N=-1$: The integral in Eq. (20), taken over the two-dimensional sphere embracing one of the point singularities in the three-dimensional $(\mathbf{k}/k_F,x)$ space, is equal to $N=-1$. As a result, the real order parameter $\mathbf{d}$ should deviate from the unit vector in the vicinity of the singularity and tend to zero for $x=0$. Thus the gap in the quasiparticle spectrum E

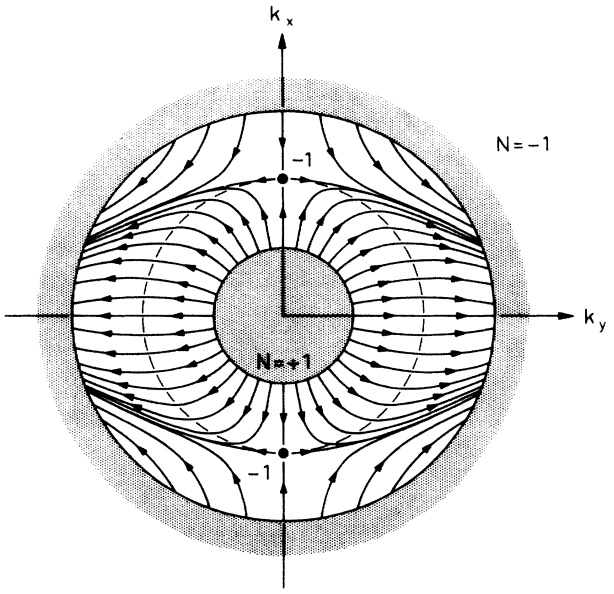

FIG. 7. The distribution of the field $\mathbf{d}(\mathbf{k},x)=\mathbf{d}(\mathbf{r})$ in the $(\mathbf{k},x)$ space of Fig. 6 for solution 1 in Fig. 1. There are two singular points ("hedgehogs") for $x=0$ at $\mathbf{k}=\pm k_F\hat{\mathbf{x}}$, both with the topological charge $N=-1$, which undo the transition from the $x\to+\infty$ vacuum

$$\begin{bmatrix}+1&0&0\\0&+1&0\\0&0&+1\end{bmatrix}$$

into the $x\to-\infty$ vacuum

$$\begin{bmatrix}-1&0&0\\0&+1&0\\0&0&+1\end{bmatrix}$$

with the different topological charges: $N=+1$ and $N=-1$, correspondingly. Displayed is the $(\hat{\mathbf{k}}_x,\hat{\mathbf{k}}_y)$ projection of the sphere; in the present case the instanton is *axisymmetric* about $\hat{\mathbf{k}}_x$, such that the whole object can easily be pictured in the third dimension as a surface of revolution.

$$E^2 \cong v_F^2(k_x \pm k_F)^2 + [A_{yy}(x=0)]^2(k_y^2+k_z^2) + \left[\frac{\partial A_{xx}}{\partial x}(x=0)\right]^2 k_F^2 x^2 , \quad (21)$$

reduces to zero inside the domain wall at $x=0$, and this occurs only for the two points on the Fermi sphere with $\mathbf{k}=\pm k_F\hat{\mathbf{x}}$ [Eq. (21) expresses E^2 in the vicinity of the two point singularities]. Thus $E=0$ at two points in the four-dimensional $(\mathbf{k},x)$ space. The order-parameter structure at $x=0$ corresponds to the so-called "planar" superfluid pairing state.[1]

Figure 8 displays the corresponding topology for the $C_\pi^{(S)y}e^{i\pi}$ wall (or for the $C_\pi^{(S)z}e^{i\pi}$ wall). In this case, the pair of singularities has rotated into the direction $\hat{\mathbf{k}}_y$ perpendicular to $\hat{\mathbf{k}}_x$. Figure 9 correspondingly shows the topologies for the $C_\pi^{(S)z}$ and $C_\pi^{(S)y}$ walls, which have the same topological charges $N=+1$ on both sides of the wall. There occur in these cases a node on a ring (that we would call a "myriapod") around the Fermi sphere. Note the broken continuous axisymmetry of the ring node, with the remaining discrete rotational symmetry C_2. Figure 10 illustrates, however, an axisymmetric ring node, realized for the wall $C_\pi^{(S)x}$. A ring node is a topologically unstable disclination loop, with the trivial topological charge $N=0$, corresponding to the "polar" pairing state[1] for the superfluid ^{3}He at $x=0$.

Figure 11 shows the spontaneous breaking of the maximally symmetric state for the pure phase-slip wall $e^{i\pi}$, which is unstable towards bifurcation into the two walls: $C_\pi^{(S)x}e^{i\pi}$ and $C_\pi^{(S)x}$. The whole Fermi sphere of zeros in the gap corresponds to the normal state, ^{3}He-N, at $x=0$ [Fig. 11(a)]. During the splitting, it transforms into a pair of point singularities, accompanied with a string: the ring node [see Fig. 11(b)]. The remaining composite topological object, nevertheless, retains axisymmetry.

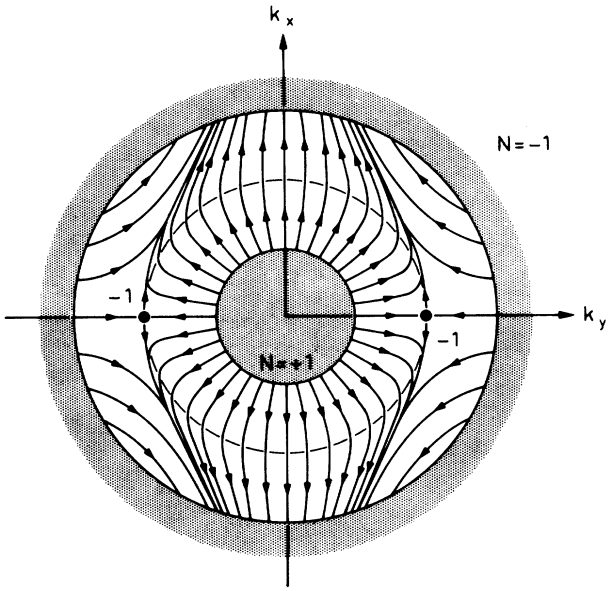

FIG. 8. As in Fig. 7, but for solution 2 (or number 3, upon the replacement $\hat{\mathbf{y}}\leftrightarrow\hat{\mathbf{z}}$) in Fig. 1. Unlike Fig. 7, this instanton provides an example of *broken axisymmetry* in the $(\mathbf{k},\mathbf{r})$ space: the solution is not rotationally symmetric about the axis $\hat{\mathbf{k}}_y$, along which the point singularities at $x=0$ here occur for $\mathbf{k}=\pm k_F\hat{\mathbf{y}}$, both with $N=-1$. The singular points in this instanton realize the transformation from the $x=+\infty$ vacuum with $N=+1$,

$$\begin{bmatrix} +1 & 0 & 0 \\ 0 & +1 & 0 \\ 0 & 0 & +1 \end{bmatrix},$$

into the vacuum for $x=-\infty$ with $N=-1$,

$$\begin{bmatrix} +1 & 0 & 0 \\ 0 & -1 & 0 \\ 0 & 0 & +1 \end{bmatrix}.$$

The walls 2 and 3 are degenerate in zero magnetic field, but a finite field serves to lift this degeneracy.

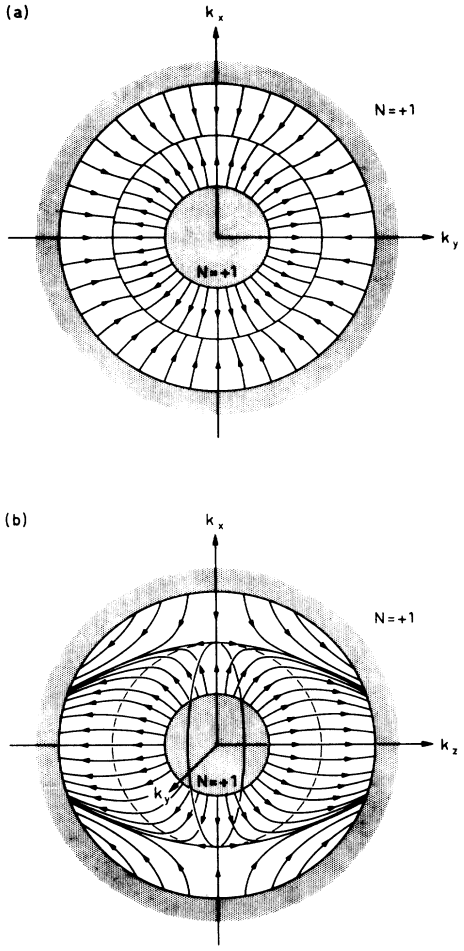

FIG. 9. Same as in Fig. 7, but in two different projections for the *nonaxisymmetric* solution 4 (and for 5, upon the interchange $\hat{\mathbf{y}}\leftrightarrow\hat{\mathbf{z}}$) of Fig. 1. (a) In the $(\hat{\mathbf{k}}_x,\hat{\mathbf{k}}_y)$ plane, instead of a point singularity ("hedgehog"), the solution exhibits a circular node for $x=0$ on a ring at the equator, a nonaxisymmetric ring node ("myriapod"), with the topological charge $N=0$, which in this case possesses only discrete symmetry C_2 upon a rotation through π about the axis $\hat{\mathbf{k}}_z$. (b) The $(\hat{\mathbf{k}}_x,\hat{\mathbf{k}}_z)$ projection of the same object shows the ring extending into the third dimension.

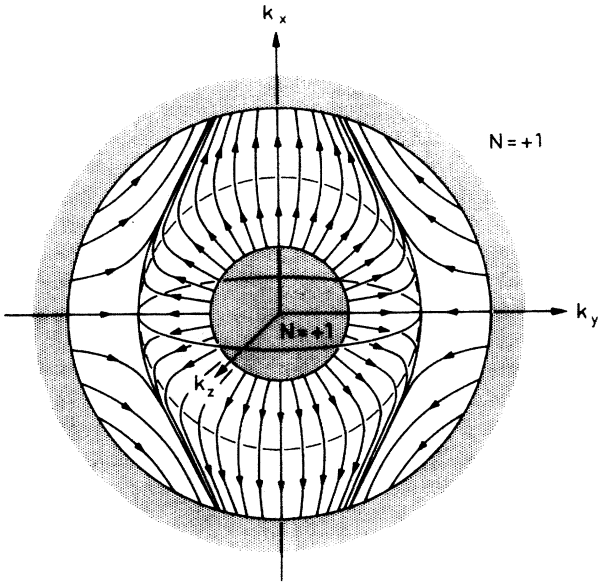

FIG. 10. The same as in Fig. 9, but for solution 6. This case exhibits full rotational symmetry C_∞ about the $\hat{\mathbf{k}}_x$ axis. The *axisymmetric* ring node—with $N=0$—occurs in the cross-sectional $(\hat{\mathbf{k}}_y,\hat{\mathbf{k}}_z)$ plane.

V. INSTANTON IN (k,r) SPACE: A NEW DIABOLICAL POINT

The point within the four-dimensional $(\mathbf{k},\mathbf{r})$ space where the fermionic energy spectrum $E(\mathbf{k},x)=[\varepsilon_k^2+\mathbf{d}^2(\mathbf{k},x)]^{1/2}$ tends towards zero, serves to provide an example of diabolical points occurring in condensed-matter and particle theory, which play a crucial role in the quantum dynamics. The diabolical points[11] are exclusive points in the spectrum of the dynamical system in the sense that at these points the usual energy-level anticrossing rule of quantum mechanics is violated, i.e., the contact of two branches of the spectrum with the same symmetry may take place.[12]

The particular points where the two branches are in contact are topologically stable: they are described by a topological charge;[13,14] therefore, they cannot be destroyed by a continuous deformation of the spectrum. If the two branches which cross each other at the diabolical points correspond to particles and holes with energies having opposite signs—then, in the diabolical points, the fermionic energy reaches to zero, i.e., the fermionic *zero modes* occur, which are stable towards the perturbations. These give rise to several profound anomalies encountered both within condensed-matter and elementary-particle physics.

The more commonly examined diabolical points[11] have the codimensions $n=2$ or $n=3$ (the codimension n of a diabolical point is defined as the dimension of the space of parameters where the pointlike contact of the different branches of the energy spectrum occurs). However, several more complicated diabolical points with higher codimensions are also possible for prescribed symmetries of the Hamiltonian matrix, and they are described[15] by the homotopic groups π_{n-1}.

Let us first discuss the familiar case of the diabolical points featuring the codimension $n=3$ in superfluid ^{3}He. This means the points in the three-dimensional $\mathbf{k}$ space where the different branches of the Hamiltonian 4×4 matrix, Eq. (14), encounter a contact. Such points are defined as topological defects described by the homotopy

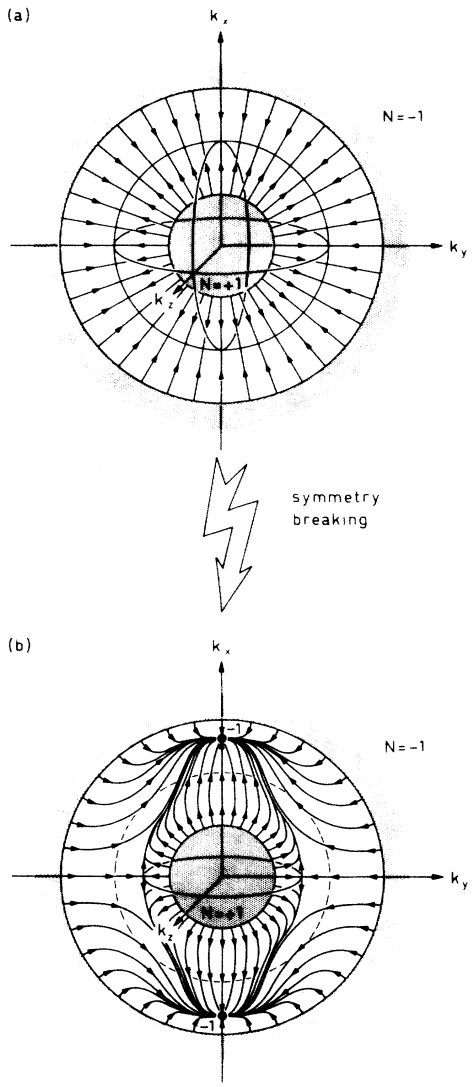

FIG. 11. The *symmetry-breaking scenario* for the saddle-point solution 7 in Fig. 1. (a) For the $e^{i\pi}$ wall in the maximally symmetric possible state, the symmetry $Pe^{i\pi}$ requires the simultaneous vanishing of all the order-parameter components, $A_{xx}(x=0)\equiv A_{yy}(x=0)\equiv A_{zz}(x=0)\equiv0$ at $x=0$ and, consequently, a node surface around the Fermi sphere at $x=0$, i.e., this wall (Ref. 10) would have a normal core (^{3}He-N) at $x=0$, with the gap amplitude vanishing on the whole Fermi sphere. (b) Solution 7 has spontaneously decayed into two domain walls, 6 and 1. The symmetry $Pe^{i\pi}$ is broken in this process, but *axisymmetry* remains (such as in the constituent solutions 1 and 6 as well, see Figs. 7 and 10) about $\hat{\mathbf{k}}_x$: the sphere S^2 has disintegrated into a pair of point singularities in the directions $\mathbf{k}=\pm k_F\hat{\mathbf{x}}$, and a node ring on a circle S^1 contained in the cross-sectional $(\hat{\mathbf{k}}_y,\hat{\mathbf{k}}_z)$ plane.

group $\pi_2(R)$, where R stands for the manifold of 4×4 matrices with all eigenvalues being distinct,[14] which is topologically equivalent to the manifold

$$R=\mathrm{U}(4)/\mathrm{U}(1)\times\mathrm{U}(1)\times\mathrm{U}(1)\times\mathrm{U}(1) \tag{22}$$

[or, what is equivalent: $R=\mathrm{SU}(4)/\mathrm{U}(1)\times\mathrm{U}(1)\times\mathrm{U}(1)$]. Since $\pi_2(R)=Z\times Z\times Z$, such topologically nontrivial points can indeed exist. Moreover, if the symmetry is favorable, these points should be realized just on the Fermi surface, where the positive-energy quasiparticle spectrum touches the negative-energy quasihole spectrum.

Near such a diabolical point $\mathbf{k}_0$, the Hamiltonian (14) reduces into a 2×2 matrix, describing the two crossing degenerate branches in touch, quasiparticles and quasiholes, and obtains the following general form:

$$\hat{\mathbf{H}}=\boldsymbol{\sigma}\cdot\mathbf{m}(\mathbf{k}),\quad m_\alpha(\mathbf{k})=e^i_\alpha(k_i-k_{0,i})\ . \tag{23}$$

In the semiclassical representation, as the coefficients e^i_α and the position $\mathbf{k}_0$ of the diabolical point become $\mathbf{r}$ dependent, and in the further quantum generalization as $\mathbf{k}\to\nabla/i$, Eq. (23) corresponds to the Hamiltonian of a chiral massless fermion moving in the electromagnetic field $\mathbf{A}=\mathbf{k}_0(\mathbf{r},t)$ and in the gravitational field specified by the triads $e^i_\alpha(\mathbf{r},t)$ ($g^{ij}=\sum_\alpha e^i_\alpha e^j_\alpha$ defines the metric tensor).

Consequently, the massless Fermi excitations in superfluid ^{3}He and the chiral Weyl fermions in quantum electrodynamics share a common origin: the topologically stable diabolical point with the codimension $n=3$ in the $\mathbf{k}$ space. This is a source of the close analogy[6] between the anomalous dynamics of superfluid ^{3}He-A, where two such diabolical points exist on the Fermi surface (also referred to as the "boojums on the Fermi surface"[4,5]), and anomalies in the $3+1$ quantum electrodynamics with Weyl fermions. Note, however, that—as distinct from elementary-particle physics—the usual problems of a quantum-field theory, such as the chiral anomaly and the vacuum polarization, can here be solved completely since in ^{3}He-A one knows the ultraviolet asymptotics and there occurs absolutely no need to introduce an unknown cutoff.

The instantons in the $(\mathbf{k},\mathbf{r})$ space, i.e., the analogues to the "cosmic" vacuum interfaces in superfluid ^{3}He-B, produce novel examples of diabolical points featuring a higher codimension, namely $n=4$. The topological origin for such a point is the additional symmetry of the Hamiltonian in Eq. (14)—due to the field $\mathbf{d}(\mathbf{k},\mathbf{r})$ being real in the domain wall. The space R of the 4×4 matrix $\hat{\mathbf{H}}(\mathbf{k},\mathbf{r})$ in Eq. (14) with a real $\mathbf{d}$ field is

$$R(\text{real }\mathbf{d})=\mathrm{SU}(2)\ , \tag{24}$$

with $\pi_2(R)=0$ and $\pi_3(R)=Z$. Such symmetry excludes the possibility of topologically stable diabolical points with $n=3$—since $\pi_2(R)=0$—but, because $\pi_3(R)$ is nontrivial, it nevertheless admits the existence of the diabolical points displaying the new—and higher—codimension $n=4$, i.e., for the branches' point of contact to occur in a four-dimensional space.

It is easy to verify that the point defects in the four-dimensional $(\mathbf{k},x)$ space found in Sec. IV correspond to diabolical points having $n=4$; namely, the integral over a three-dimensional sphere S^3 in the $(\mathbf{k},x)$ space, embracing the point:

$$N=\frac{1}{48\pi^2}\int_{S^3\text{ around instanton}} dS_\mu\,\epsilon^{\mu\nu\alpha\beta}\,\mathrm{Tr}(U^\dagger\partial_\nu U)(U^\dagger\partial_\alpha U)(U^\dagger\partial_\beta U) \tag{25}$$

is unity. Here U is the unitary matrix diagonalizing the Hermitian matrix $\hat{\mathbf{H}}$ [Eq. (14), with real $\mathbf{d}$].

The general form of the fermionic Hamiltonian in the vicinity of the diabolical point with $n=4$ produces a new generic class of Hamiltonians in condensed-matter and particle physics. This class contains, in particular, the Dirac Hamiltonian (below, α and β are 4×4 Dirac matrices):

$$\hat{\mathbf{H}}=\boldsymbol{\alpha}\cdot\mathbf{k}+\beta m\ , \tag{26}$$

with a diabolical point occurring at $\mathbf{k}=0$, $m=0$ in the four-dimensional $(\mathbf{k},m)$ space. Thus the fermionic dynamics near the instanton in the $(\mathbf{k},x)$ space found in the previous section is analogous to the fermionic dynamics in the domain wall within the quantum-field theory of Dirac fermions, whose mass m vanishes at $x=0$.

The fermionic zero modes are also responsible for the spontaneous spin supercurrent in the cosmiclike ^{3}He-B domain walls at $T=0$ (near T_c, this supercurrent was calculated in the Ginzburg-Landau approximation in Sec. III). The exact spectrum of the fermions in the wall may be found in a quantum-mechanical treatment[16] of the Hamiltonian in Eq. (14). There exist two asymmetric branches of the fermionic spectrum in the wall—one for each spin projection—see Figs. 12, which intersect the energy-level zero, i.e., the Fermi surface. The fermions occupying the negative levels in any one of these branches serve to produce the net ground-state mass current. The mass currents carried by both branches exactly compensate each other, thus,

$$j_y=\sum k_y(n_\uparrow+n_\downarrow)=0\ . \tag{27}$$

However, the spin currents of both branches add up, hence producing the sum total spontaneous ground-state spin supercurrent

$$j^z_y=\sum k_y(n_\uparrow-n_\downarrow)\neq0\ . \tag{28}$$

This is here seen to be a direct consequence of the breaking of the discrete symmetry in the cosmiclike B-B vacuum interface.

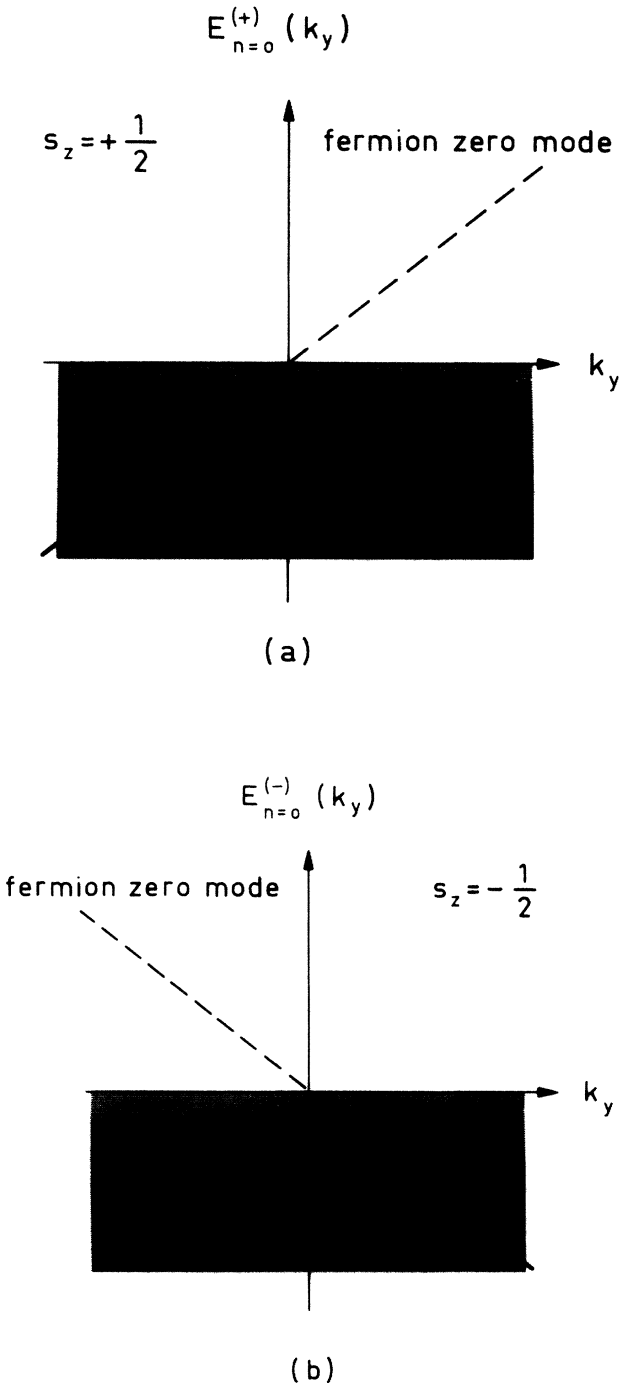

FIG. 12. Schematic illustration of the dispersion relation for the fermion energy spectrum in the cosmiclike ^{3}He-B domain wall for both branches of the spectrum, as a function of k_y—the wave vector within the plane of the interface—for k_y tending towards zero. (a) For spin $s = \uparrow$; (b) for spin $s = \downarrow$. The spectrum displays a diabolical point at the crossing of the fermionic zero modes for the midgap energy (for full details of the quantum-mechanical calculations, see Ref. 16). The occurrence of these zero modes leads to a finite density of states at zero temperature; the fermions occupying the negative-energy levels of the asymmetric branches (solid lines in the figure) produce the ground-state spin supercurrent, while the mass supercurrent is exactly compensated.

The same situation occurs inside the cores of quantized vortices in superfluid ^{3}He, where the breaking of parity spontaneously produces either spin or mass supercurrents in the core along the vortex axis.[5] An analogous symmetry breaking has been postulated to occur also in the hypothetical "superconducting" cosmic strings,[17] in such a manner that there will arise a spontaneous electric current along the string axis.

The massless fermions can exist only in the plane $x = 0$, while outside this plane the fermions necessarily acquire a finite mass. Therefore, the B-B vacuum interfaces, as well as the quantized vortices[5] in ^{3}He, serve to provide intrigueing analogies—within condensed-matter physics—to the concept of *space compactification*. Note that the linear objects in superfluid ^{3}He, such as vortices and disclinations, may contain diabolical points of the codimension $n = 5$, while the pointlike soliton can have diabolical points of codimension $n = 6$.

VI. DISCUSSION

In the superfluid phases of ^{3}He—including ^{3}He-B—such as within modern gauge theories of the fundamental interactions, the "vacuum" is far from being an inactive "ether." Instead, it constitutes a dynamical object, capable of occupying different ground states. The state of the vacuum and its possible inhomogeneities determine all the physical properties (such as the masses and interactions) of any particles—fermionic ^{3}He quasiparticles and/or bosonic collective modes—immersed into it. Although the vacuum assumes a ground state—that with the lowest energy—this state is by no means unique, owing to the internal degrees of freedom which specify the state of the vacuum. Therefore, there may occur B-B boundaries separating the inequivalent vacua of ^{3}He-B: nontopological domain walls, objects analogous to the domain walls in cosmology, supported by symmetry and bridging the mutually degenerate ground states.

Note that unlike the present models[8] for the postulated "cosmic domain walls" in the Higgs fields of the early Universe, the B-B vacuum interfaces considered here, owing to energy considerations, never possess a "normal" core: with all the order-parameter components vanishing simultaneously; instead, the domain walls (like the vortices[5] in ^{3}He-B) display superfluid cores. The maximally symmetric normal-core wall $e^{i\pi}$ proves to be unstable towards splitting into two walls—each with a superfluid core. This is because of the internal degrees of freedom for the vacuum state; clearly, it is not possible for the "classical" superfluid ^{4}He, which lacks such degrees of freedom, to have superfluid-core domain walls.

Within gauge-field theories, instantons represent tunneling solutions in imaginary time[7] between topologically different vacua; in the present context the instantons are realized in the $(\mathbf{k},x)$ space, and represent tunneling solutions in x space between topologically different $\mathbf{k}$-space vacua. However, the tunneling solution obtained through substitution of the real-space coordinate x to imaginary time is also possible: in this case the diabolical points will occur in the four-dimensional $(\mathbf{k},t)$ space. It will be of interest to examine whether these elusive objects in space or time—inhomogeneities of the vacuum—

can be verified experimentally. In order to produce the B-B domain walls in the laboratory frame, consider:

(i) The outcome of a rapid pressurization scheme depicted in Fig. 13. Essentially, this is equivalent to the "Kibble scenario" for the formation of domain structures in a spontaneously broken gauge theory,[18] first suggested in the cosmological context. Note that while the cosmological theories generating domain walls can probably be eliminated because of their unacceptable gravitational effects, a network of domain walls can be generated in superfluid ^{3}He-B, as suggested in the caption of Fig. 13.

(ii) Alternatively, one may conceive nucleating superfluid ^{3}He in the B phase confined to a tube divided by a wall: once both sides of the wall reside in the B phase the wall is removed, thus possibly introducing the B-B domain boundary in the sample, provided that the two sides occupy disparate vacua. Reflections of these walls in a sample volume could be seen in the propagation of ultrasound through the cell.

(iii) The domain walls can also be emitted by moving objects, such as the hypercooled superfluid A-B phase boundary,[19] in particular. This emission process can become the most prominent dissipation mechanism for superflow decay at low temperatures, where the friction force due to the scattering of the ^{3}He quasiparticle excitations off the A-B interface may be neglected, since the thermal excitations tend to become rapidly frozen out. Combined objects, bound states of the A-B phase boundary, and an accompanying B-B domain wall, have been found;[20] moreover, the critical velocities at which emission of the B-B walls occur were calculated in Ref. 20 for the moving A-B interface (these very same B-B vacuum interfaces were referred to as "interphasons" in Ref. 20), i.e., since in a cooldown one *a priori* cannot fix the phase of the superfluid condensate, one would expect that in one-half of the experimental realizations of the superfluid A-B interface, the phase boundary would be a one-core structure, while the two-core structure—the bound state of an A-B interface with a B-B interface—is equally likely. The moving A-B phase boundary becomes unstable towards the emission of the B-B vacuum interfaces at a finite propagation velocity, thus giving rise to the generation of these structures in the bulk superfluid.

Experimentally, the occurrence of the domain walls in superfluid ^{3}He is further complicated due to the existence of the two length scales, ξ_{GL} and ξ_D, in the domain-wall structure (analogously to the hard- and soft-core structures of vortices in ^{3}He). However, since for small magnetic fields one has $\xi_D \gg \xi_{GL}$, the structure in these different core regimes is in this case independent of each other. The topologically stable domain walls due to the dipole interaction ("soft" core) may contain inner nontopological cosmiclike domain walls (i.e., a "hard" core), in which the mutual orientation of the order parameter in the domains (see Sec. III) is not determined by the dipole interaction, but rather is due to the symmetry of the vacuum alone. Within the soft dipole core, the superfluid is in the B-phase state (whose orientation is just rotated),

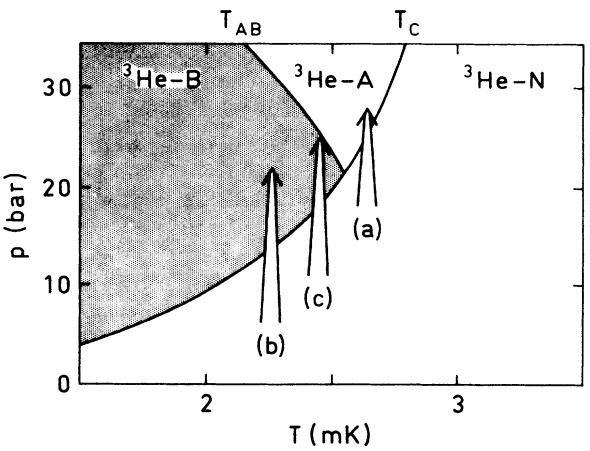

FIG. 13. A sudden pressurization of normal ^{3}He Fermi liquid, ^{3}He-N, from just below T_c into the superfluid state, may be carried out (a) into ^{3}He-A, (b) into ^{3}He-B, or (c) onto the superfluid ^{3}He A-B coexistence curve. Here we are interested in the possibility to generate, as the outcome, causally disjoint nucleation centers of ^{3}He-B (separated spatially by distances $d \gg \xi_{GL}$, a condition equivalent to "cosmic inflation") in different vacuum states. At the interfaces for domains in the inequivalent vacua, it is possible to encounter actual experimental realizations of the different cosmiclike B-B boundaries introduced in the present paper. (See Ref. 18 for further details.)

while, in contrast, in the hard core the ^{3}He-B state is broken (while retaining superfluidity everywhere) in one of the two possible ways found necessary for a plane of phase slippage in bulk ^{3}He-B: through the formation of the polar or planar states, respectively.

In the future, we investigate the magnetic-field dependence of the B-B interfacial energies, in order to study the lifting of the degeneracy of the domain walls; in high fields it will also be of special interest to consider the interaction of the hard core of the domain wall, which we have considered in detail above, with the soft dipole core. In addition, it is motivated to study moving B-B interfaces, where, like for the moving A-B boundary,[20] the loss of time-reversal invariance (T) may radically alter the structure of the walls and their relative energies due to the dispersion relation as a function of the propagation velocity for the front. We have recently found[21] related A-A vacuum interfaces also in the superfluid A phase.

ACKNOWLEDGMENTS

One of us (M.M.S.) is grateful to Professor H. E. Hall, Professor K. Kajantie, and Professor O. V. Lounasmaa; the other (G.E.V.) to Professor S. P. Novikov for useful discussions. This research has been supported through funding for the Advancement of European Science from the Körber Foundation and by the project ROTA between the Soviet Academy of Sciences and the Academy of Finland.

[1]For reviews on the superfluid phases of ^{3}He, see, A. J. Leggett, Rev. Mod. Phys. **47**, 331 (1975); J. C. Wheatley, *ibid.* **47**, 415 (1975); P. W. Anderson and W. F. Brinkman, in *The Physics of Liquid and Solid Helium, Part II,* edited by K. H. Bennemann and J. B. Ketterson (Wiley, New York, 1978), Chap. 3; D. M. Lee and R. C. Richardson, *ibid.*, Chap. 4.

[2]For comprehensive reviews on topological defects in condensed matter, see, N. D. Mermin, Rev. Mod. Phys. **51**, 591 (1979); V. P. Mineev, in *Soviet Scientific Reviews A2,* edited by I. M. Khalatnikov (Harwood Academic, Chur, Switzerland, 1980), p. 173; M. Kléman, *Points, Lines and Walls in Liquid Crystals, Magnetic Systems and Various Ordered Media* (Wiley, New York, 1983).

[3]The symmetry of defects in condensed matter is discussed in M. M. Salomaa and G. E. Volovik, Phys. Rev. Lett. **51**, 2040 (1983); Phys. Rev. B **31**, 203 (1985); Phys. Rev. Lett. **54**, 2127 (1985); A. A. Balinskiĭ, G. E. Volovik, and E. I. Kats, Zh. Eksp. Teor. Fiz. **87**, 1305 (1984) [Sov. Phys.—JETP **60**, 748 (1984)], and Ref. 5.

[4]On the momentum-space topology in ^{3}He, see, G. E. Volovik and V. P. Mineev, Zh. Eksp. Teor. Fiz. **83**, 1025 (1982) [Sov. Phys.—JETP **56**, 579 (1982)]; M. M. Salomaa and G. E. Volovik, Europhys. Lett. **2**, 781 (1986), and Ref. 5.

[5]M. M. Salomaa and G. E. Volovik, Rev. Mod. Phys. **59**, 533 (1987).

[6]The analogy between superfluid ^{3}He-A dynamics and quantum-field theory, including the chiral anomaly, is developed in G. E. Volovik, Pis'ma Zh. Eksp. Teor. Fiz. **43**, 428 (1986) [JETP Lett. **43**, 551 (1986)]; **43**, 535 (1986) [**43**, 693 (1986)]; **44**, 144 (1986) [**44**, 185 (1986)]; **44**, 388 (1986) [**44**, 498 (1986)]; for a review, see, G. E. Volovik, J. Low Temp. Phys. **67**, 331 (1987).

[7]S. Coleman, *Aspects of Symmetry* (Cambridge University Press, Cambridge, 1985); see, in particular, Chap. 8.

[8]On cosmic strings and cosmic domain walls, see, Ya. B. Zel'dovich, I. Yu. Kobzarev, and L. B. Okun, Zh. Eksp. Teor. Fiz. **67**, 3 (1974) [Sov. Phys.—JETP **67**, 401 (1975)]; T. W. B. Kibble, Phys. Rep. **67**, 183 (1980); A. Vilenkin, *ibid.* **121**, 263 (1985), and Ref. 17.

[9]V. P. Mineev and G. E. Volovik, Phys. Rev. B **18**, 3197 (1978).

[10]V. L. Golo and M. I. Monastyrsky, Phys. Lett. **66A**, 302 (1978).

[11]M. V. Berry and M. Wilkinson, Proc. R. Soc. London, Ser. A **392**, 15 (1984); M. V. Berry, *ibid.* **392**, 45 (1984).

[12]J. von Neumann and E. P. Wigner, Phys. Z. **30**, 465 (1929); *ibid.* **30**, 467 (1929).

[13]S. P. Novikov, Dokl. Akad. Nauk SSSR **257**, 538 (1981).

[14]J. E. Avron, R. Seiler, and B. Simon, Phys. Rev. Lett. **51**, 51 (1983).

[15]G. E. Volovik, Pis'ma Zh. Eksp. Teor. Fiz. **46**, 81 (1987) [JETP Lett. **46**, 98 (1987)].

[16]M. M. Salomaa and G. E. Volovik (unpublished).

[17]E. Witten, Nucl. Phys. **B249**, 557 (1985).

[18]T. W. B. Kibble, J. Phys. A **9**, 1387 (1976).

[19]For the moving superfluid ^{3}He A-B phase boundary, see, D. S. Buchanan, G. W. Swift, and J. C. Wheatley, Phys. Rev. Lett. **57**, 341 (1986); S. Yip and A. J. Leggett, *ibid.* **57**, 345 (1986).

[20]M. M. Salomaa, J. Phys. C (to be published).

[21]M. M. Salomaa and G. E. Volovik, J. Low Temp. Phys. (to be published).

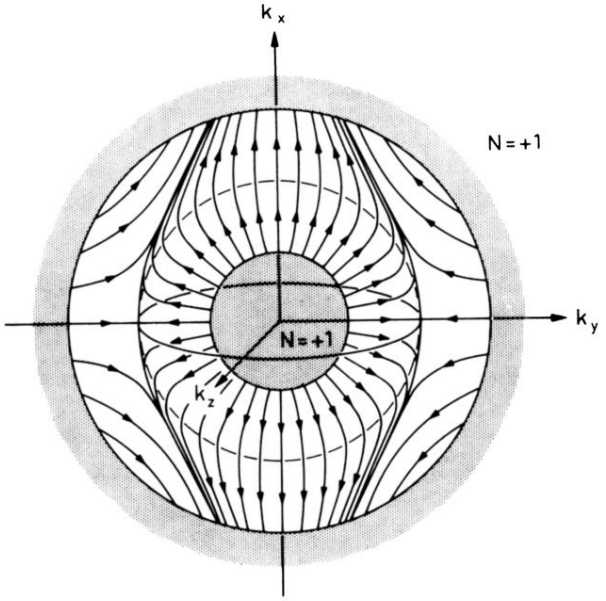

FIG. 10. The same as in Fig. 9, but for solution 6. This case exhibits full rotational symmetry C_∞ about the $\hat{\mathbf{k}}_x$ axis. The *axisymmetric* ring node—with $N=0$—occurs in the cross-sectional $(\hat{\mathbf{k}}_y, \hat{\mathbf{k}}_z)$ plane.

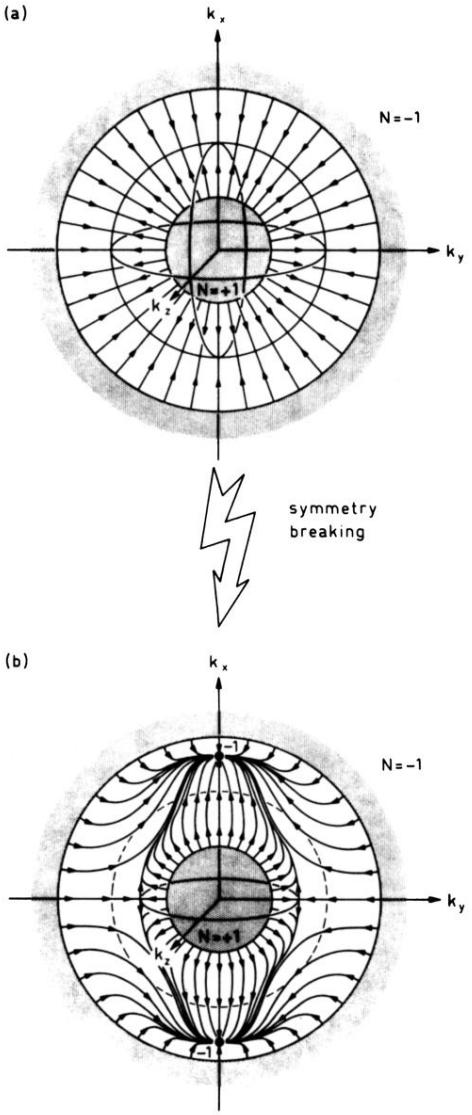

FIG. 11. The *symmetry-breaking scenario* for the saddle-point solution 7 in Fig. 1. (a) For the $e^{i\pi}$ wall in the maximally symmetric possible state, the symmetry $Pe^{i\pi}$ requires the simultaneous vanishing of all the order-parameter components, $A_{xx}(x=0) \equiv A_{yy}(x=0) \equiv A_{zz}(x=0) \equiv 0$ at $x=0$ and, consequently, a node surface around the Fermi sphere at $x=0$, i.e., this wall (Ref. 10) would have a normal core (^{3}He-N) at $x=0$, with the gap amplitude vanishing on the whole Fermi sphere. (b) Solution 7 has spontaneously decayed into two domain walls, 6 and 1. The symmetry $Pe^{i\pi}$ is broken in this process, but *axisymmetry* remains (such as in the constituent solutions 1 and 6 as well, see Figs. 7 and 10) about $\hat{\mathbf{k}}_x$: the sphere S^2 has disintegrated into a pair of point singularities in the directions $\mathbf{k} = \pm k_F \hat{\mathbf{x}}$, and a node ring on a circle S^1 contained in the cross-sectional $(\hat{\mathbf{k}}_y, \hat{\mathbf{k}}_z)$ plane.

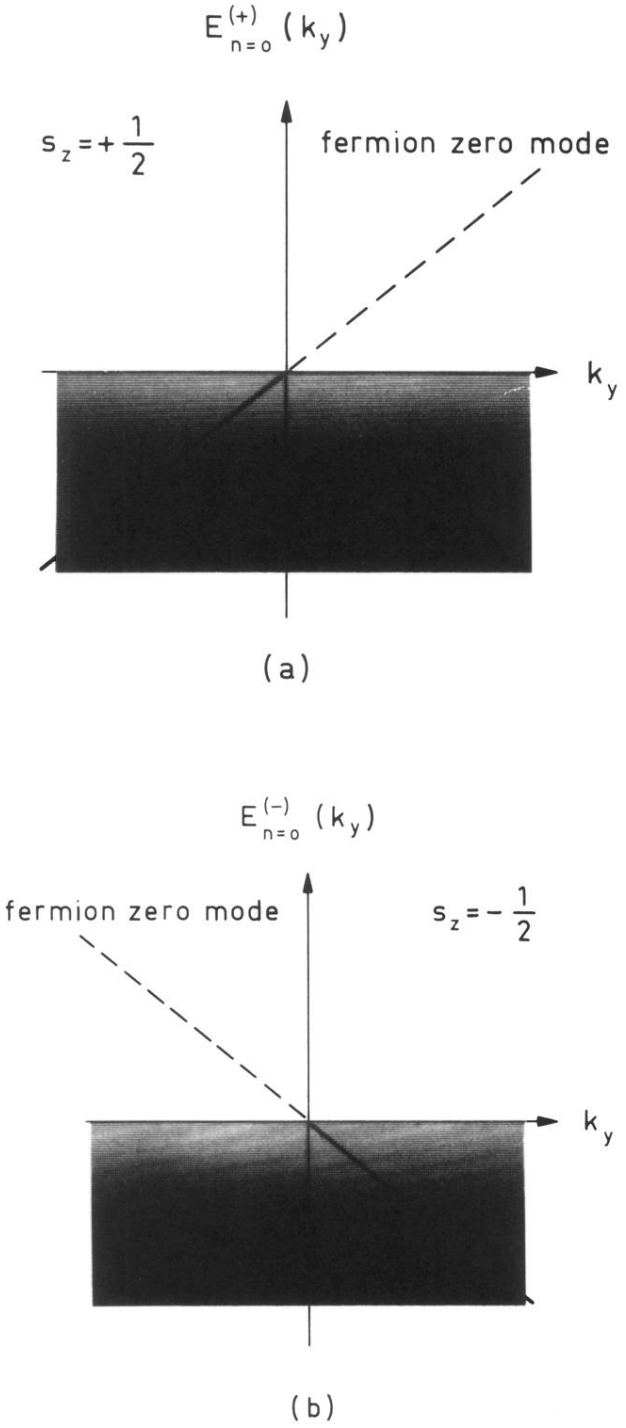

FIG. 12. Schematic illustration of the dispersion relation for the fermion energy spectrum in the cosmiclike ^{3}He-B domain wall for both branches of the spectrum, as a function of k_y—the wave vector within the plane of the interface—for k_y tending towards zero. (a) For spin $s = \uparrow$; (b) for spin $s = \downarrow$. The spectrum displays a diabolical point at the crossing of the fermionic zero modes for the midgap energy (for full details of the quantum-mechanical calculations, see Ref. 16). The occurrence of these zero modes leads to a finite density of states at zero temperature; the fermions occupying the negative-energy levels of the asymmetric branches (solid lines in the figure) produce the ground-state spin supercurrent, while the mass supercurrent is exactly compensated.

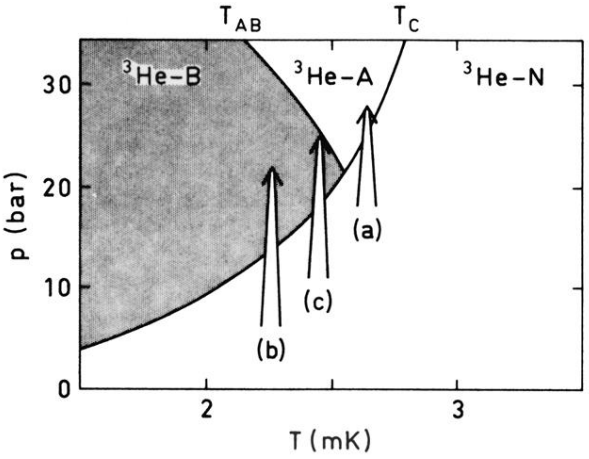

FIG. 13. A sudden pressurization of normal ^{3}He Fermi liquid, ^{3}He-N, from just below T_c into the superfluid state, may be carried out (a) into ^{3}He-A, (b) into ^{3}He-B, or (c) onto the superfluid ^{3}He A-B coexistence curve. Here we are interested in the possibility to generate, as the outcome, causally disjoint nucleation centers of ^{3}He-B (separated spatially by distances $d \gg \xi_{GL}$, a condition equivalent to "cosmic inflation") in different vacuum states. At the interfaces for domains in the inequivalent vacua, it is possible to encounter actual experimental realizations of the different cosmiclike B-B boundaries introduced in the present paper. (See Ref. 18 for further details.)

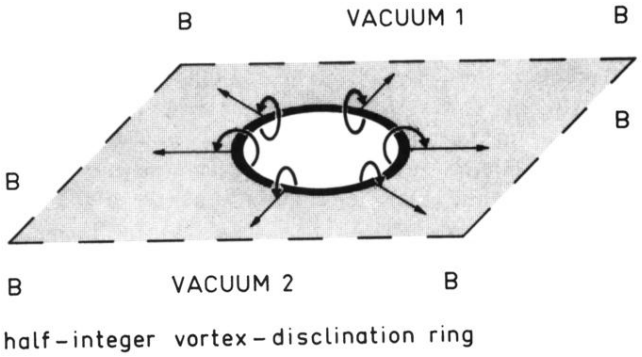

FIG. 4. The instanton between separate B-phase vacua can display a hole, bounded by a ring. Depending on the type of the domain wall, the ring will be a half-quantum vortex ring (for the $e^{i\pi}$ wall), a half-integer spin-disclination ring (e.g., for the boundary $C_{\pi}^{(S)x}$), or a simultaneous half-quantum vortex and a half-integer disclination ring (e.g., for $C_{\pi}^{(S)x}e^{i\pi}$). Once formed, and with its radius first exceeding several coherence lengths, the ring spontaneously expands out. While the ring propagates radially outward it serves to extinguish the domain wall.

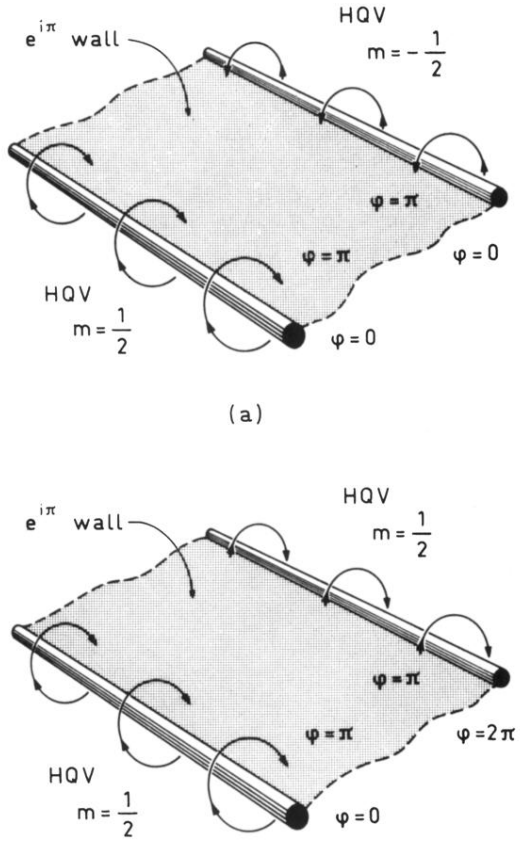

FIG. 5. The vacuum interfaces in ^{3}He-B represent planes of phase slippage, which may terminate in linear defects. Illustrated here are such edges of the domain walls involving half-quantum vortices (HQV) that carve the $e^{i\pi}$ domain wall from distinct B-phase vacua. (a) The two HQV's have opposite circulation: $m = \frac{1}{2}$ and $m = -\frac{1}{2}$. (b) The HQV's both share the same number of circulation quanta, $m = \frac{1}{2}$.

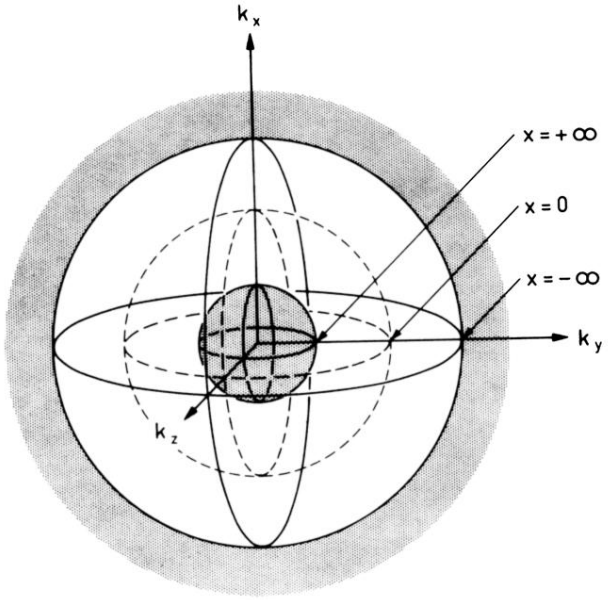

FIG. 6. The three-dimensional $(\mathbf{k},x)$ space is homeomorphic to a solid sphere enclosing a hole. The x-axis maps into r, the radial coordinate; the two-dimensional (2D) Fermi surfaces of $\mathbf{k}$ ($\mathbf{k}$ is restrained to lie on the Fermi sphere, and should thus be considered 2D) at each x maps onto a spherical surface with the corresponding r. For the mapping between the points $\mathbf{r}$ of the solid sphere and the coordinates $\mathbf{k}$ and x we use the relation $\mathbf{r}=(\mathbf{k}/|\mathbf{k}|)[1-\frac{1}{2}\tanh(x/5\xi_{\mathrm{GL}})]$, through Figs. 7–10 (in Fig. 11, x is scaled by $7.5\xi_{\mathrm{GL}}$).

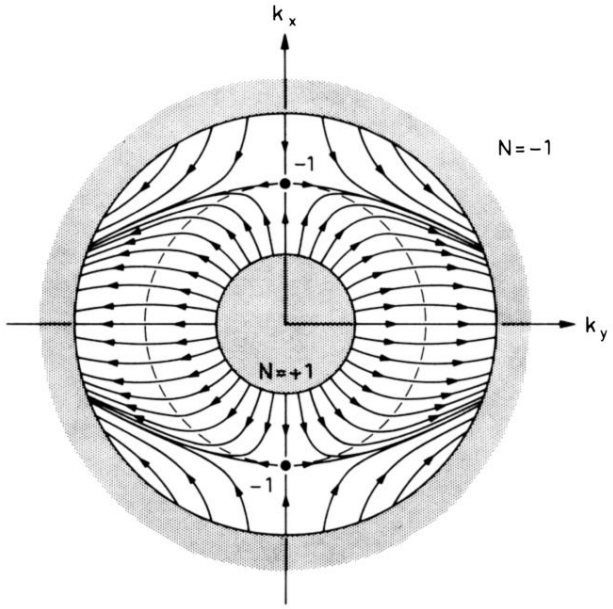

FIG. 7. The distribution of the field $\mathbf{d}(\mathbf{k},x)=\mathbf{d}(\mathbf{r})$ in the $(\mathbf{k},x)$ space of Fig. 6 for solution 1 in Fig. 1. There are two singular points ("hedgehogs") for $x=0$ at $\mathbf{k}=\pm k_F\hat{\mathbf{x}}$, both with the topological charge $N=-1$, which undo the transition from the $x\rightarrow+\infty$ vacuum

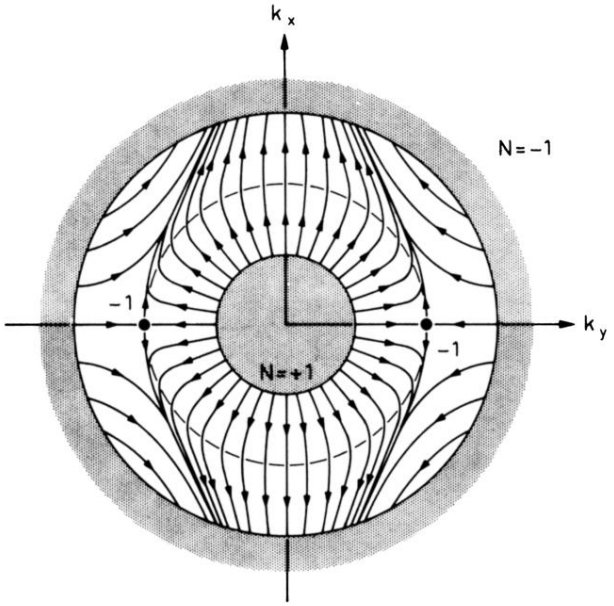

FIG. 8. As in Fig. 7, but for solution 2 (or number 3, upon the replacement $\hat{\mathbf{y}} \leftrightarrow \hat{\mathbf{z}}$) in Fig. 1. Unlike Fig. 7, this instanton provides an example of *broken axisymmetry* in the $(\mathbf{k},\mathbf{r})$ space: the solution is not rotationally symmetric about the axis $\hat{\mathbf{k}}_y$, along which the point singularities at $x=0$ here occur for $\mathbf{k}=\pm k_F\hat{\mathbf{y}}$, both with $N=-1$. The singular points in this instanton realize the transformation from the $x=+\infty$ vacuum with $N=+1$,

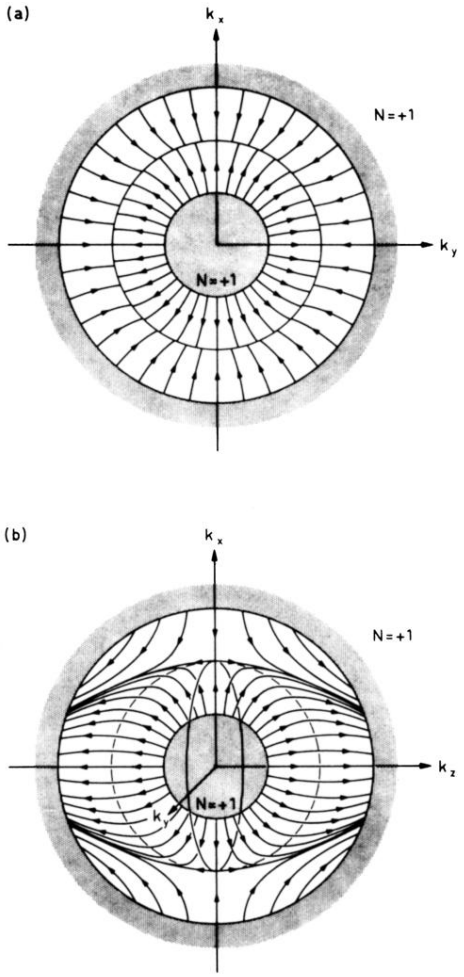

FIG. 9. Same as in Fig. 7, but in two different projections for the *nonaxisymmetric* solution 4 (and for 5, upon the interchange $\hat{\mathbf{y}} \leftrightarrow \hat{\mathbf{z}}$) of Fig. 1. (a) In the $(\hat{\mathbf{k}}_x, \hat{\mathbf{k}}_y)$ plane, instead of a point singularity ("hedgehog"), the solution exhibits a circular node for $x = 0$ on a ring at the equator, a nonaxisymmetric ring node ("myriapod"), with the topological charge $N = 0$, which in this case possesses only discrete symmetry C_2 upon a rotation through π about the axis $\hat{\mathbf{k}}_z$. (b) The $(\hat{\mathbf{k}}_x, \hat{\mathbf{k}}_z)$ projection of the same object shows the ring extending into the third dimension.